

Probing quantum chaos in multipartite systems

Zan Cao¹, Zhenyu Xu¹, and Adolfo del Campo^{2,3}

¹School of Physical Science and Technology, Soochow University, Suzhou 215006, China

²Department of Physics and Materials Science, University of Luxembourg, L-1511 Luxembourg, Luxembourg

³Donostia International Physics Center, E-20018 San Sebastián, Spain

Understanding the emergence of quantum chaos in multipartite systems is challenging in the presence of interactions. We show that the contribution of the subsystems to the global behavior can be revealed by probing the full counting statistics of the local, total, and interaction energies. As in the spectral form factor, signatures of quantum chaos in the time domain dictate a dip-ramp-plateau structure in the characteristic function, i.e., the Fourier transform of the eigenvalue distribution. With this approach, we explore the fate of chaos in interacting subsystems that are locally maximally chaotic. Global quantum chaos can be suppressed at strong coupling, as illustrated with coupled copies of random-matrix Hamiltonians and of the Sachdev-Ye-Kitaev model. Our method is amenable to experimental implementation using single-qubit interferometry.

Identifying signatures of chaos in the quantum domain remains a nontrivial task in complex systems [1]. Quantum chaos has manifold applications and appears in different fields involving the study of many-body complex quantum systems [2–4], statistical mechanics of isolated quantum systems [5, 6], anti-de Sitter black holes [7–11], holographic quantum matter [12], and quantum information science [13, 14], among other examples. Several diagnostic tools for quantum chaos have been proposed. They include the spectral form factor (SFF) [1], fidelity decay [15], Loschmidt echo (LE) [16], out-of-time-order correlator (OTOC) [17], quantum circuit complexity [18, 19], etc. Connections among these diagnostics have been explored in specific areas ranging from many-body systems to quantum field theory [16, 20–24]. More recently, diagnostics of quantum chaos have been extended to open systems to account for the effect of decoherence and dissipation [25–36].

A prominent signature of quantum chaos is the repulsion among energy levels. For instance, the spacing between nearest-neighbor levels follows the Wigner-Dyson distribution in quantum chaotic systems, while it is described by Poisson statistics in the presence of conserved quantities (e.g., in integrable systems) [37]. The SFF is proportional to $|Z(\beta + it)|^2$, where $Z(\cdot)$ is the partition function and $\beta = 1/k_B T$. This quantity probes the level statistics of both close and far-separated energy eigenvalues, providing a tool to detect the ergodic nature of the system [1]. For a generic chaotic system, the SFF exhibits a dip-ramp-plateau structure. Its short-time decay forms a slope. The physical origin of the subsequent ramp is the long-range repulsion between energy levels [11]. The transition from the slope to the ramp forms the dip. The final plateau originates from the finite Hilbert space dimension and approaches a constant value $Z(2\beta)$ in the absence of degeneracies in the energy spectrum. The SFF has been widely employed in the study of the discrete energy spectrum of quantum chaotic systems [11, 38–44].

Quantum systems composed of multipartite subsystems subject to generic interactions typically have a complex energy spectrum. We shall focus on a global subsystem composed of strongly-chaotic subsystems, interacting with each other. In this setting, any subsystem can be seen as an open quantum system embedded in an environment, composed of the remaining subsystems. The subsystem dynamics is thus governed by dissipative quantum chaos [1], which is currently under exhaustive study [28, 29, 32, 33, 36, 45–49]. We shall depart from the standard practice of assuming an effective open quantum dynamics, as ubiquitously done in the literature. Instead, we will account for the exact unitary dynamics of the global composite system, with no approximations

Zhenyu Xu: zhenyuxu@suda.edu.cn

Adolfo del Campo: adolfo.delcampo@uni.lu

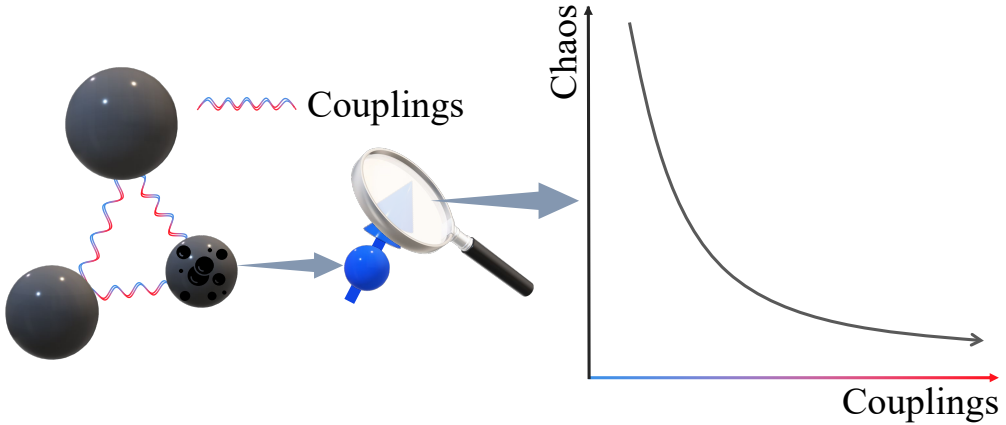


Figure 1: **Schematic picture.** The emergence of quantum chaos in multipartite systems can be revealed by probing the full counting statistics of the local, total, and interaction energies with an ancillary qubit. Global quantum chaos could be suppressed at strong couplings.

(e.g., without invoking the Markovian description or an effective master equation.). The above diagnostics can be employed to detect global quantum chaos in multipartite systems [50]. However, they are not suited to detect how chaotic behavior stems from the subsystems and their interactions, see Fig. 1. In this work, we provide an experimentally realizable approach to this end by considering the measurement of an energy observable X , which can be the Hamiltonian of a subsystem or the interaction energy. As measurement outcomes are stochastic, we propose to study the full counting statistics, characterized by the eigenvalue distribution of X at thermal equilibrium. Its Fourier transform, the characteristic function, reveals chaotic behavior through the dip-ramp-plateau structure. Its analysis shows that strong interactions among the different subsystems can suppress the global chaotic behavior of the multipartite system, even when the subsystems are maximally chaotic, as revealed by the study of global and local observables. This scheme not only provides a convenient theoretical tool to diagnose quantum chaos in complex multipartite quantum systems, but it can be experimentally realized by using single-qubit interferometry with an ancillary qubit.

1 The characteristic function of the energy observable X

Let $\mathcal{H} = \bigotimes_l \mathcal{H}_l$ be the Hilbert space of a multipartite system and X be an energy observable of a local subsystem in the subspace $\bigotimes_k \mathcal{H}_k \subseteq \mathcal{H}$. We focus on the Hamiltonian of the subsystems (local energy) and the interaction energy, as choices of the observable X . The probability distribution of the observable X with eigenvalues $\{x\}$ averaged over an initial state ρ_0 is [51]

$$P(x) = \text{tr} [\rho_0 \delta(X - x)]. \quad (1)$$

The eigenvalue probability distribution $P(x)$ encodes the full counting statistics of the observable X , that is, the probability to find the system in an eigenstate with eigenvalue x when prepared in the state ρ_0 . In terms of the integral representation of the Dirac delta function, the probability distribution can be expressed as the Fourier transform

$$P(x) = \frac{1}{2\pi} \int_{-\infty}^{+\infty} g(t) e^{-itx} dt, \quad (2)$$

of the characteristic (moment generating) function

$$g(t) = \text{tr} (\rho_0 e^{itX}), \quad (3)$$

that captures the statistical properties of the spectrum of the observable X . While in the following we refer to t as a time variable, it is to be understood as the Fourier conjugate to x . We note that

that the complex conjugate obeys $g(t)^* = g(-t)$. Further, provided that the total Hamiltonian H and the operator X are both time-reversal symmetric, it follows that $g(t) = g(-t)$, i.e., $g(t)$ is a real function.

Experimentally, the characteristic function Eq. (3) can be measured by introducing an auxiliary qubit coupled to the system. This technique known as single-qubit interferometry has been widely used in measuring form factors of Floquet operators [52], fidelity decay [26], LE [53, 54], work statistics [55–57], Lee-Yang zeros [58–60], OTOC [61], quantum-state reconstruction of dark systems [62], full distribution of many-body observables [51], and SFF [63]. The key procedure is to perform a controlled X gate conditioning on the auxiliary qubit, i.e.,

$$U(t) = |1\rangle\langle 1| \otimes \exp(itX) + |0\rangle\langle 0| \otimes \mathbb{1}. \quad (4)$$

This allows us to recover the real and imaginary parts of Eq. (3) by measuring a pair of Pauli operators on the ancillary qubit [51], i.e., $\text{Re}(g(t)) = \text{tr}(\sigma_z \rho_{\text{ancillary}})$ and $\text{Im}(g(t)) = \text{tr}(\sigma_y \rho_{\text{ancillary}})$, where $\rho_{\text{ancillary}} = \text{tr}_{\text{system}}(H \otimes \mathbb{1} U(t) |+\rangle\langle +| \otimes \rho_0 U^\dagger(t) H \otimes \mathbb{1})$, H is the Hadamard gate, and $|+\rangle = (|0\rangle + |1\rangle)/\sqrt{2}$.

2 A diagnostic for quantum chaos in multipartite systems

In what follows, we consider the absolute square value of the generating function in Eq. (3), i.e.,

$$G(t) = |g(t)|^2 = |\text{tr}(\rho_0 e^{itX})|^2, \quad t \in [0, \infty), \quad (5)$$

as a tool for probing quantum chaos in multipartite systems, identifying contributions from the subsystems and their interactions. The choice $X = H_j$ represents the local energy that can be employed to diagnose the chaotic behavior contributed by the j th subsystem in an N -partite system. By contrast, the observable $X = H_j \otimes H_k \otimes H_l$ can be used to detect signature of quantum chaos attributed to the interactions among subsystems j , k , and l .

The original motivation behind Eq. (5) is based on the fact that when the observable X is chosen as the global Hamiltonian $X = H$ ($H \in \mathcal{H}$) and the initial state is in thermal equilibrium, i.e., $\rho_0 = \rho_{\text{th}} = e^{-\beta H}/Z(\beta)$, the absolute square value of the generating function in Eq. (5) turns out to be $G(t) = \left| \frac{Z(\beta+it)}{Z(\beta)} \right|^2$, which equals the SFF [11, 22, 64] and can be interpreted as the fidelity between the initial coherent Gibbs state (or a thermofield double state) and the state resulting from its evolution [33, 43]. In addition, when X is a small perturbation of the Hamiltonian H , i.e., $H = H_0 + X$, and commutes with H (or H_0), Eq. (5) is also equivalent to the LE $G(t) = |\langle \psi_0 | e^{itH} e^{-itH_0} | \psi_0 \rangle|^2$, which captures the overlap between two identical initial states ($\rho_0 = |\psi_0\rangle\langle\psi_0|$) evolving under slightly different Hamiltonians H and H_0 [16]. Note that according to the Baker–Campbell–Hausdorff formula, Eq. (5) and the LE differ in the general case, when $[X, H] \neq 0$.

We emphasize that the observable X in Eq. (5) is not required to represent a small perturbation or to commute with H . When it describes the local energy of a subsystem $\bigotimes_k \mathcal{H}_k \subseteq \mathcal{H}$, Eq. (5) provides the possibility to directly detect the chaotic behavior contributed by the subsystems or interactions to the global multipartite system. It can be used to either diagnose quantum chaos of a one-partite system (as done by the SFF) or a structured multipartite system. To support this observation, we illustrate its use in the following examples involving coupled random-matrix Hamiltonians and the coupled SYK model.

3 Probing the transition from chaos to nonchaotic behavior in coupled random-matrix Hamiltonians

Consider a N -partite system with a general Hamiltonian of the form

$$H = \sum_{j=1}^N H_j^{(0)} + \epsilon_1 \sum_{j < k=2}^N H_j^{(1)} \otimes H_k^{(1)} + \dots + \epsilon_{N-1} \bigotimes_{j=1}^N H_j^{(N-1)}, \quad (6)$$

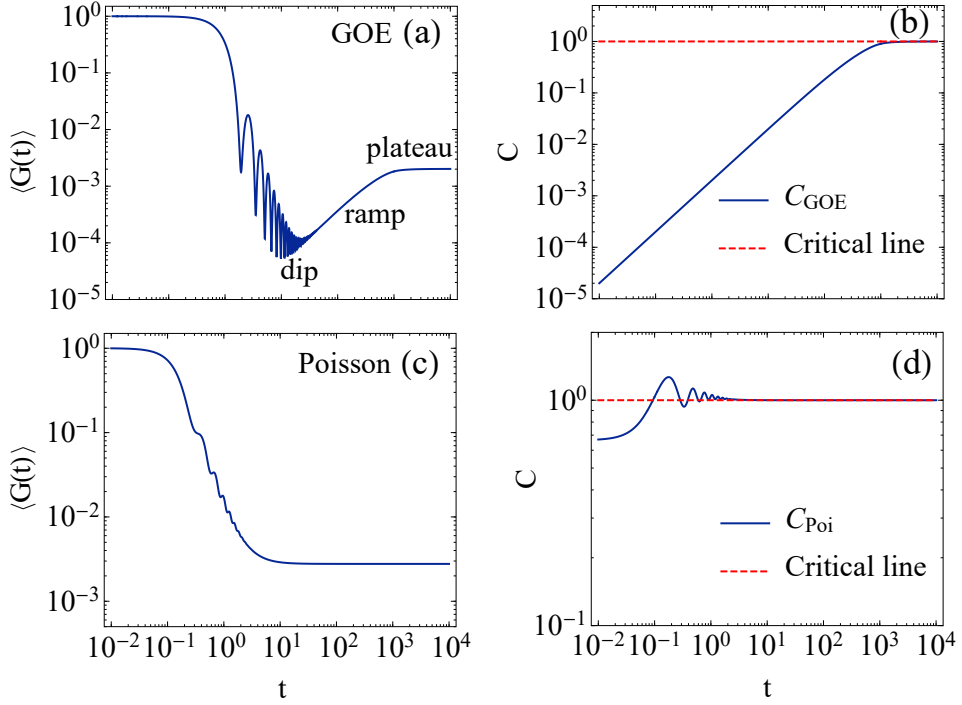


Figure 2: **The generating function $G(t)$ for the total energy distribution averaged over the GOE and Poisson statistics.** Analytical Eq. (9) is depicted in (a) with $\beta = 0.1$ and $d = 500$. The standard deviation of the random variables of H is selected as $\sigma = 1/\sqrt{d}$. The dip-ramp-plateau structure in (a) reflects a typical feature for chaotic systems, which is due to the anticorrelation of the energy spectrum with $C < 1$ ($t > t_{\text{dip}}$) as shown in (b). In comparison, non-chaotic Poisson statistics of $\langle G(t) \rangle$ (Eq. (12)) and C (Eq. (13)) are depicted in (c) and (d).

where $H_j^{(0)}$ is the Hamiltonian of the j th subsystem and ϵ_{l-1} is the coupling constant for the l -partite interaction $\bigotimes_{j=1}^l H_j^{(l-1)}$. In the annealing approximation, the eigenvalue correlations of an arbitrary observable X can be defined by

$$C = \frac{\langle G(t) \rangle - |\langle g(t) \rangle|^2}{\langle G(\infty) \rangle}. \quad (7)$$

In specific, when $X = H$ and $\rho_0 = \rho_{\text{th}}$, Eq. (7) reduces to

$$C = \frac{\langle |Z(\beta + it)|^2 \rangle - |\langle Z(\beta + it) \rangle|^2}{\langle Z(2\beta) \rangle}, \quad (8)$$

assuming no degeneracies in the spectrum of H . Negative values of the quantity $\langle |Z(\beta + it)|^2 \rangle - |\langle Z(\beta + it) \rangle|^2 - \langle Z(2\beta) \rangle$ indicate that the eigenvalues are anticorrelated, and the value $C = 1$ turns out to be the critical one, i.e., signatures of quantum chaos imply $C < 1$ ($t \gg 1$).

For the sake of illustration, let us sample the Hamiltonians from the Gaussian orthogonal ensemble (GOE) [2, 65], which is a paradigmatic random matrix ensemble for physical applications involving systems with time-reversal symmetry and exhibiting quantum chaos. GOE is the ensemble of real symmetric matrices, whose elements are chosen at random from a Gaussian distribution. The joint probability density of $H_j \in \text{GOE}(d_j)$ (d_j denotes the dimension of the Hilbert space \mathcal{H}_j) is proportional to $\exp(-\frac{1}{2\sigma^2} \text{tr} H_j^2)$, where σ is the standard deviation of the random matrix elements of H_j .

The first example we consider is the one-partite case, i.e., $N = 1$. In this scenario, $X = H \in \text{GOE}(d)$ and Eq. (5) averaged over GOEs yields (see Appendix)

$$\langle G(t) \rangle_{\text{GOE}} \doteq \frac{\langle Z(2\beta) \rangle_{\text{GOE}} \cdot C_{\text{GOE}} + |\langle Z(\beta + it) \rangle_{\text{GOE}}|^2}{\langle Z(\beta) \rangle_{\text{GOE}}^2}, \quad (9)$$

where \doteq denotes the annealing approximation. In Eq. (9), the GOE averaged partition function is given by

$$\langle Z(x) \rangle_{\text{GOE}} = \frac{\sqrt{d} I_1(2\sigma\sqrt{d}x)}{\sigma x}, \quad (10)$$

where $I_n(\cdot)$ is the modified Bessel function of first kind and order n , and the coefficient reads

$$C_{\text{GOE}} = \begin{cases} \frac{t\sigma}{\sqrt{d}} - \frac{t\sigma}{2\sqrt{d}} \ln \left(1 + \frac{t\sigma}{\sqrt{d}} \right), & t \leq 2\sqrt{d}/\sigma, \\ 2 - \frac{t\sigma}{2\sqrt{d}} \ln \frac{t+\sqrt{d}/\sigma}{t-\sqrt{d}/\sigma}. & t > 2\sqrt{d}/\sigma. \end{cases} \quad (11)$$

As shown in Fig. 2 (a), Eq. (9) exhibits a typical feature of quantum chaos, namely a dip-ramp-plateau structure. The early decay from unit value comes to an end, forming a dip (also known as correlation hole) with the onset of a ramp. The latter extends until it saturates at a plateau value at the characteristic plateau time $t_{\text{plateau}} = 2\sqrt{d}/\sigma$ [see Eq. (11)]. The existence of the ramp, a period of linear growth of $\langle G(t) \rangle_{\text{GOE}}$, is a consequence of the repulsion between long-range energy levels [11]. This long-range repulsion causes the energy levels to be anticorrelated [see in Fig. 2 (b), where $C_{\text{GOE}} < 1$ before the plateau time] and therefore to be lower than the plateau. The plateau stems from the discrete energy spectrum, whose height is $\langle Z(2\beta) \rangle_{\text{GOE}} / \langle Z(\beta) \rangle_{\text{GOE}}^2$. Similar chaotic features have been studied in the Gaussian Unitary Ensemble (GUE) [33, 43, 66], Gaussian ensembles under infinite temperature [67], and Sachdev–Ye–Kitaev (SYK) models [11, 68, 69].

In comparison, a non-chaotic system with energy levels distributed by Poisson distribution $p(E_k, k) = \frac{e^{-\frac{E_k}{\sigma}}}{\sigma(k-1)!} \left(\frac{E_k}{\sigma} \right)^{k-1}$ [70] will have no dip-ramp-plateau structure. The ensemble averaged Eq. (5) and coefficient Eq. (7) are obtained by

$$\langle G(t) \rangle_{\text{Poi}} \doteq \frac{\langle Z(2\beta) \rangle_{\text{Poi}} \cdot C_{\text{Poi}} + |\langle Z(\beta + it) \rangle_{\text{Poi}}|^2}{\langle Z(\beta) \rangle_{\text{Poi}}^2}, \quad (12)$$

and

$$C_{\text{Poi}} = 1 + \frac{\eta - |\langle Z(\beta + it) \rangle_{\text{Poi}}|^2}{\langle Z(2\beta) \rangle_{\text{Poi}}}, \quad (13)$$

respectively, where the partition function is denoted by

$$\langle Z(x) \rangle_{\text{Poi}} = \frac{1 - (1 + x\sigma)^{-d}}{\sigma x}, \quad (14)$$

with $\eta = \frac{1 - g_+^{1-d} - g_-^{1-d} + (1 + 2\beta\sigma)^{1-d}}{\sigma^2(t^2 + \beta^2)}$, and $g_{\pm} = 1 + \sigma(\beta \pm it)$.

As shown in Fig. 2 (c), Eq. (12) will monotonically (except some revivals in the slope) decrease to $\langle Z(2\beta) \rangle_{\text{Poi}} / \langle Z(\beta) \rangle_{\text{Poi}}^2$ with no dip-ramp-plateau structure. In such scenario, the anticorrelation parameter C_{Poi} always approaches 1 in the same time period of the dip-plateau time region as in the GOE case, illustrating that no chaotic behavior exists in this context.

Without loss of generality, we then consider a bipartite system with $H_{1,2}^{(0)} = H_{1,2}^{(1)}$ and $H_{1,2}^{(0)} \neq H_{1,2}^{(1)}$ in two scenarios. Since $H_{1,2}^{(0,1)}$ are independently sampled from GOEs, $H_{1,2}^{(0)} = H_{1,2}^{(1)}$ ensures $[H, X] = 0$, while $H_{1,2}^{(0)} \neq H_{1,2}^{(1)}$ guarantees $[H, X] \neq 0$. As illustrated in Fig. 3, the use of $G(t)$ as a diagnostic tool is applicable whether $[H, X] = 0$ or $[H, X] \neq 0$.

As the total system is composed of two partitions each described by a random-matrix Hamiltonian, it is not surprising that in the absence of (or weak) interactions the full system exhibits the dip-ramp-plateau structure when choosing $X = H$ [dark blue curves in Fig. 3 (a) and (e)]. However, when the coupling strength ϵ_1 between subsystems 1 and 2 is enhanced, the dip-ramp-plateau structure gradually washes out and finally disappears [light blue curves in Fig. 3 (a) and (e)]. This is because the anticorrelation of the energy spectrum is weakened when enhancing the coupling [see in Fig. 3 (b) and (f)], implying that the interactions between subsystems might have a great impact on the chaotic dynamics of the system as a whole.

To account for this phenomenon, in Fig. 3 (c), we look at the characteristic function for different choices of the observable $X = H_1^{(0)}$ and $X = H_1^{(0)} \otimes H_2^{(0)}$ [$X = H_1^{(1)} \otimes H_2^{(1)}$]. Fig. 3 (c) and (g)

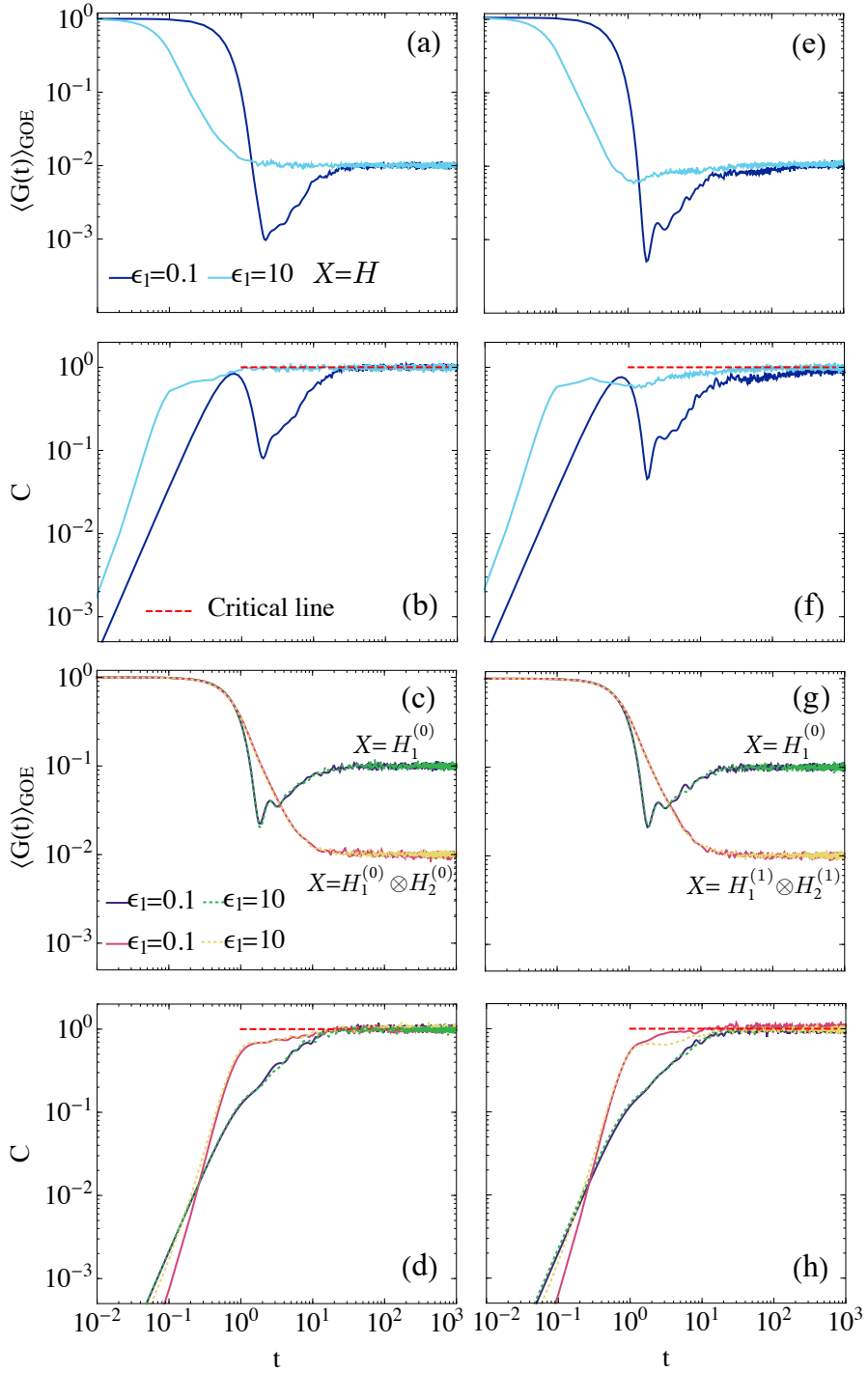


Figure 3: Transition from chaotic to non-chaotic regimes in a bipartite system. Left column: $H = H_1^{(0)} + H_2^{(0)} + \epsilon_1 H_1^{(0)} \otimes H_2^{(0)}$. (a) Equation (5) averaged over GOEs for observables $X = H$ with coupling strength $\epsilon_1 = 0.1$ and 10 respectively. $H_1^{(0)}$ and $H_2^{(0)}$ are sampled from GOE independently, with 500 realizations, $d_1 = d_2 = 10$, and $\beta = 0.01$. A chaotic to non-chaotic transition takes place when the coupling constant ϵ_1 is enhancing. (b) The coefficient C as function of time, compared with critical line $C = 1$ for $X = H$. $C < 1$ signals anticorrelation among energy levels. (c) The GOE averaged $G(t)$ is depicted with $X = H_1^{(0)}$ and $X = H_1^{(0)} \otimes H_2^{(0)}$, respectively, in which $H_1^{(0)} \otimes H_2^{(0)}$ with no dip-ramp-plateau structure plays an important role in cancelling the chaotic behavior. (d) The coefficient C as function of time, compared with critical line $C = 1$ for $X = H_1^{(0)}$ and $X = H_1^{(0)} \otimes H_2^{(0)}$, respectively. Panels in the right column (e)–(h) mirror those in the left for $H = H_1^{(0)} + H_2^{(0)} + \epsilon_1 H_1^{(1)} \otimes H_2^{(1)}$ and $H_{1,2}^{(0)} \neq H_{1,2}^{(1)}$.

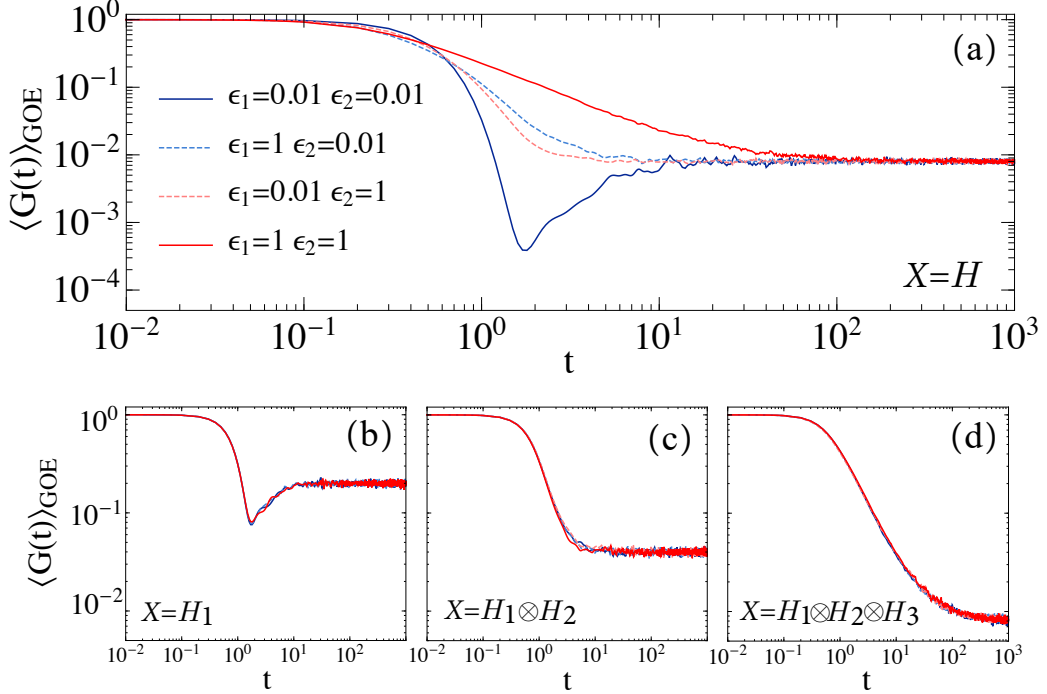


Figure 4: **Transition across chaotic and non-chaotic regimes in a tripartite system.** Equation (5) averaged with GOEs for observables (a) $X = H$, (b) $X = H_1$, (c) $X = H_1 \otimes H_2$, and (d) $X = H_1 \otimes H_2 \otimes H_3$, respectively. H_1 , H_2 , and H_3 are sampled from GOE independently, with 500 realizations, $d_1 = d_2 = d_3 = 5$, and $\beta = 0.01$.

show how these choices identify the contributions to quantum chaos by the first subsystem and the interactions between subsystems 1 and 2. Obviously, $H_1^{(0,1)} \otimes H_2^{(0,1)}$ plays an important role in cancelling the chaotic behavior, since the characteristic function reflects no ramp structure, i.e., the long-range anticorrelations. Indeed, from the perspective of nearest-neighbor level distribution, the Kronecker product of random matrices as a whole will tend toward Poisson statistics [71]. When the coupling is enhanced, the interaction term $H_1^{(0,1)} \otimes H_2^{(0,1)}$ dominates, and the whole system gradually transits from a chaotic to a non-chaotic regime.

Similar phenomena exist in more structured systems, as shown in Fig. 4 for a tripartite system. For simplicity, we only consider $H_{1,2,3}^{(0)} = H_{1,2,3}^{(1)} = H_{1,2,3}^{(2)}$ and omit the superscript therein. Both bipartite interactions (e.g., $H_1 \otimes H_2$), and the tripartite interaction $H_1 \otimes H_2 \otimes H_3$ play an important role in canceling the quantum chaotic behavior of the composite global system, while the local chaotic nature of each subsystem can be detected by choosing a local observable (e.g. $X = H_1$) even at strong coupling.

It is worth to note that the presence of interactions could also induce chaos if the interaction tend to mix the subsystems, just as shown in the coupled kicked rotors [72].

4 Coupled Sachdev-Ye-Kitaev model

The second example we consider is the coupled Sachdev-Ye-Kitaev (cSYK) model [73–82]. A system composed of $2N$ Majorana fermions is divided into two separated sides and each subsystem is described by the SYK model [83, 84]. We consider the left and right SYK Hamiltonians $H_{L,R}$ with a bilinear coupling H_b . The total Hamiltonian of the cSYK model reads

$$\begin{aligned}
 H &= H_L + H_R + \mu H_b \\
 &= \sum_{\alpha=L,R} \sum_{1 \leq k < l < m < n \leq N} J_{klmn} \chi_k^\alpha \chi_l^\alpha \chi_m^\alpha \chi_n^\alpha + \mu i \sum_{k=1}^N K_{kk} \chi_k^L \chi_k^R,
 \end{aligned} \tag{15}$$

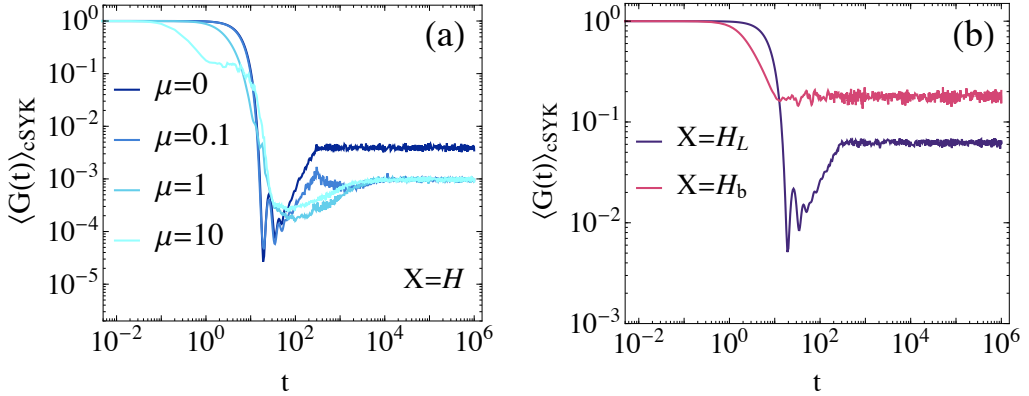


Figure 5: **Chaotic behavior in a coupled Sachdev-Ye-Kitaev (cSYK) model.** Equation (5) averaged with cSYK for observables (a) $X = H$, (b) $X = H_L$, and $X = H_b$, respectively. The Hamiltonian is sampled by 500 realizations with $2N = 20$, $\beta = 0$, and $J = K = 1$.

where μ controls the strength of the bilinear coupling and χ_k denote Majorana fermion operators satisfying the anticommutation relations $\{\chi_k, \chi_l\} = \delta_{kl}$. J_{klmn} and K_{kk} are random coupling constants independently sampled from Gaussian distributions with zero expectation values and $\langle J_{klmn}^2 \rangle = \frac{3J^2}{N^3}$, $\langle K_{kk}^2 \rangle = \frac{K^2}{N^2}$. A similar model has been used to study the holographic duality of an eternal traversable wormhole: By preparing the SYK model in a thermofield double state and turning on the coupling between the two sides, the wormhole is traversable in the context of gravity [76].

Fig. 5 shows the numerical result for the disorder-averaged $\langle G(t) \rangle$, in agreement with the random matrix theory. From Fig. 5(b), we see that the bilinear coupling plays an important role in controlling the chaotic behavior of the whole system, as the generating function has no dip-ramp-plateau structure. The chaotic character of the system is robust when the bilinear coupling is weak ($\mu \lesssim 0.1$). When enhancing the coupling, the dip-ramp-plateau structure of the entire system is gradually washed out [Fig. 5(a)]. This implies that the entire system becomes non-chaotic when the bilinear coupling is strong, even when the subsystems remain chaotic. As in the GOE example, the chaotic nature of each subsystem can be detected by choosing a local observable (e.g. $X = H_L$), as shown in Fig. 5(b).

5 Discussion and conclusion

We have introduced a protocol to directly diagnose quantum chaos in interacting multipartite systems by measuring the statistical distribution of an energy observable X at thermal equilibrium. Specifically, we make use of the absolute square value $G(t)$ of the generating function of the eigenvalue distribution associated with the observable X . When the observable equals the total Hamiltonian, $G(t)$ reduces to the SFF. For local observables, chaotic features give rise to a dip-ramp-plateau structure in $G(t)$, which is similar to that in SFF. $G(t)$ directly detects the contributions to quantum chaos in a composite system from different subsystems by choosing the observable for k -partite interactions. We have shown that the coupling of chaotic systems can give rise to the suppression of quantum chaos in the composite system, as the interaction strength among the subsystems is increased. In addition, even at strong coupling, the chaotic character of the subsystems can be unveiled by choosing X as a local observable, as demonstrated by considering the multipartite GOEs and the coupled SYK models.

Our scheme can be implemented in quantum devices, such as NMR systems [54, 57, 59] and trapped ions [60] by introducing an auxiliary qubit coupled to the systems, as both the random spin and SYK models are realizable in the laboratory [85–91]. Our approach for diagnosing the chaos in multipartite quantum systems may thus find broad applications in interdisciplinary studies in quantum information, quantum matter, and AdS/CFT duality, especially in analyzing quantum chaos in structured quantum many-body systems.

Acknowledgements

It is a pleasure to acknowledge discussions with Aurelia Chenu, Fernando J. Gómez-Ruiz, Mar Ferri, Wenlong You, and Yifeng Yang. This work was supported by the National Natural Science Foundation of China under Grant No. 12074280 and PAPD.

A The generating function $G(t)$ averaged over ensembles

In this appendix, we intend to briefly introduce the calculation of the generating function $G(t)$ averaged over ensembles. The averaged $G(t)$ in terms of annealing approximation is given by [33, 43]

$$\langle G(t) \rangle \doteq \frac{\langle |Z(\beta + it)|^2 \rangle}{\langle Z(\beta) \rangle^2}. \quad (16)$$

Then the denominator and numerator of Eq. (16) can be written as

$$\langle Z(\beta) \rangle = \int dE \rho(E) e^{-\beta E}, \quad (17)$$

and

$$\langle |Z(\beta + it)|^2 \rangle = \int dE \rho(E) e^{-2\beta E} + \int dE dE' \rho(E, E') e^{-(\beta + it)E} e^{-(\beta - it)E'}, \quad (18)$$

where $\rho(E)$ is the spectral density and $\rho(E, E')$ is the two-point probability density function.

A.1 Gaussian orthogonal ensemble statistics

For GOE, the spectral density and two-point probability density function are given by [33]

$$\rho(E) = \frac{1}{\sqrt{2}\sigma} \det K_d(\tilde{E}, \tilde{E}), \text{ and } \tilde{E} := \frac{E}{\sqrt{2}\sigma}, \quad (19)$$

and

$$\rho(E, E') = \frac{1}{2\sigma^2} \det \left[\begin{pmatrix} K_d(\tilde{E}, \tilde{E}) & K_d(\tilde{E}, \tilde{E}') \\ K_d(\tilde{E}', \tilde{E}) & K_d(\tilde{E}', \tilde{E}') \end{pmatrix} \right], \quad (20)$$

respectively. Note that GOE and GUE share the same form of N -point probability density function. The only difference is that the kernel $K_d(x, y)$ in Eqs. (19) and (20) for GOE is a quaternion. Note that σ is selected as $\sigma = 1/\sqrt{2}$ in Ref. [2], $\sigma = 1$ in Ref. [65], and $\sigma = 1/\sqrt{d}$ in Ref. [11], respectively. In this paper, we keep σ in the formulae for convenience.

According to Dyson's theorem [2],

$$\det A = \text{pf} (Z_N \Theta[A]), \quad (21)$$

a $N \times N$ self-dual quaternion matrix A can be represented by a $2N \times 2N$ complex matrix ($\Theta[\cdot]$ is the matrix form of a quaternion). Here pf denotes a Pfaffian and $Z_N = \bigoplus_{j=1}^N \begin{pmatrix} 0 & 1 \\ -1 & 0 \end{pmatrix}_j$. Then Eqs. (19) and (20) can be written as

$$\rho(E) = \frac{1}{\sqrt{2}\sigma} \text{pf} (Z_1 \Theta[K_d(\tilde{E}, \tilde{E})]), \quad (22)$$

and

$$\rho(E, E') = \frac{1}{2\sigma^2} \text{pf} \left(Z_2 \Theta \left[\begin{pmatrix} K_d(\tilde{E}, \tilde{E}) & K_d(\tilde{E}, \tilde{E}') \\ K_d(\tilde{E}', \tilde{E}) & K_d(\tilde{E}', \tilde{E}') \end{pmatrix} \right] \right). \quad (23)$$

The above method can be straightforwardly extended to higher point correlation functions. Similar work has been done in Ref. [67] for evaluating spectral form factors under infinite temperature.

A.2 $G(t)$ averaged by GOEs

With Eq. (22), the partition function [Eq. (17)] averaged over the GOEs is approximated by

$$\langle Z(x) \rangle_{\text{GOE}} = \frac{\sqrt{d} I_1(2\sigma\sqrt{dx})}{\sigma x}, \quad (24)$$

where $I_n(\cdot)$ is the modified Bessel function of first kind and order n (Eq. (10) in the main text).

According to Eqs. (23), the imaginary time partition function [Eq. (18)] averaged over the GOEs reads

$$\langle |Z(\beta + it)|^2 \rangle_{\text{GOE}} = \langle Z(2\beta) \rangle_{\text{GOE}} + |\langle Z(\beta + it) \rangle_{\text{GOE}}|^2 + *, \quad (25)$$

where

$$* = \begin{cases} -\frac{\alpha\sqrt{d}}{\sigma} \left[1 - \frac{t\sigma}{\sqrt{d}} + \frac{t\sigma}{2\sqrt{d}} \ln \left(1 + \frac{t\sigma}{\sqrt{d}} \right) \right], & t \leq 2\sqrt{d}/\sigma, \\ \frac{\alpha\sqrt{d}}{\sigma} \left[1 - \frac{t\sigma}{2\sqrt{d}} \ln \frac{t+\sqrt{d}/\sigma}{t-\sqrt{d}/\sigma} \right]. & t > 2\sqrt{d}/\sigma. \end{cases} \quad (26)$$

Considering $G(t)$ should be 1 when $t = 0$, α reads

$$\alpha \simeq \frac{\sigma}{\sqrt{d}} \langle Z(2\beta) \rangle_{\text{GOE}}. \quad (27)$$

Substitution of Eq. (27) and Eq. (26) into Eq. (25) together with the averaged partition function in Eq. (24), the GOE averaged $G(t)$ in Eq. (16) can be obtained straightforwardly, see Eq. (9) and Eq. (11) in the main text.

References

- [1] F. Haake, *Quantum Signatures of Chaos* (Springer, Berlin, 2010).
- [2] M. L. Mehta, *Random Matrices*, 3rd ed. (Elsevier, San Diego, 2004).
- [3] V. Zelevinsky, *Annual Review of Nuclear and Particle Science* **46**, 237 (1996).
- [4] T. Guhr, A. Müller-Groeling, and H. A. Weidenmüller, *Physics Reports* **299**, 189 (1998).
- [5] M. Srednicki, *Phys. Rev. E* **50**, 888 (1994).
- [6] L. D'Alessio, Y. Kafri, A. Polkovnikov, and M. Rigol, *Advances in Physics* **65**, 239 (2016).
- [7] P. Hayden and J. Preskill, *J. High Energy Phys.* **2007**, 120 (2007).
- [8] Y. Sekino and L. Susskind, *J. High Energy Phys.* **2008**, 065 (2008).
- [9] S. H. Shenker and D. Stanford, *J. High Energy Phys.* **2014**, 67 (2014).
- [10] J. Maldacena, S. H. Shenker, and D. Stanford, *J. High Energy Phys.* **2016**, 106 (2016).
- [11] J. S. Cotler, G. Gur-Ari, M. Hanada, J. Polchinski, P. Saad, S. H. Shenker, D. Stanford, A. Streicher, and M. Tezuka, *J. High Energy Phys.* **2017**, 118 (2017).
- [12] M. Franz and M. Rozali, *Nature Reviews Materials* **3**, 491 (2018).
- [13] P. Forrester, *Log-Gases and Random Matrices (LMS-34)*, London Mathematical Society Monographs (Princeton University Press, 2010).
- [14] S. Boixo, S. V. Isakov, V. N. Smelyanskiy, R. Babbush, N. Ding, Z. Jiang, M. J. Bremner, J. M. Martinis, and H. Neven, *Nature Physics* **14**, 595 (2018).
- [15] J. Emerson, Y. S. Weinstein, S. Lloyd, and D. G. Cory, *Phys. Rev. Lett.* **89**, 284102 (2002).
- [16] T. Gorin, T. Prosen, T. H. Seligman, and M. Znidaric, *Physics Reports* **435**, 33 (2006).
- [17] A. I. Larkin and Y. N. Ovchinnikov, *Sov. Phys. JETP* **28**, 1200 (1969).
- [18] L. Susskind, *Fortschritte der Physik* **64**, 84 (2016).
- [19] J. Cotler, N. Hunter-Jones, J. Liu, and B. Yoshida, *J. High Energy Phys.* **2017**, 48 (2017).
- [20] D. A. Roberts and B. Yoshida, *J. High Energy Phys.* **2017**, 121 (2017).
- [21] A. Chenu, I. L. Egusquiza, J. Molina-Vilaplana, and A. del Campo, *Scientific Reports* **8**, 12634 (2018).
- [22] J. Kudler-Flam, L. Nie, and S. Ryu, *J. High Energy Phys.* **2020**, 175 (2020).
- [23] B. Yan, L. Cincio, and W. H. Zurek, *Phys. Rev. Lett.* **124**, 160603 (2020).
- [24] A. Bhattacharyya, W. Chemissany, S. S. Haque, and B. Yan, *The European Physical Journal C* **82**, 1 (2022).
- [25] Z. P. Karkuszewski, C. Jarzynski, and W. H. Zurek, *Phys. Rev. Lett.* **89**, 170405 (2002).

[26] D. Poulin, R. Blume-Kohout, R. Laflamme, and H. Ollivier, *Phys. Rev. Lett.* **92**, 177906 (2004).

[27] S. V. Syzranov, A. V. Gorshkov, and V. Galitski, *Phys. Rev. B* **97**, 161114 (2018).

[28] Z. Xu, L. P. García-Pintos, A. Chenu, and A. del Campo, *Phys. Rev. Lett.* **122**, 014103 (2019).

[29] A. del Campo and T. Takayanagi, *J. High Energy Phys.* **2020**, 170 (2020).

[30] J. Tuziemski, *Phys. Rev. A* **100**, 062106 (2019).

[31] B. Yoshida and N. Y. Yao, *Phys. Rev. X* **9**, 011006 (2019).

[32] L. Sá, P. Ribeiro, and T. Prosen, *Phys. Rev. X* **10**, 021019 (2020).

[33] Z. Xu, A. Chenu, T. Prosen, and A. del Campo, *Phys. Rev. B* **103**, 064309 (2021).

[34] P. Zanardi and N. Anand, *Phys. Rev. A* **103**, 062214 (2021).

[35] N. Anand, G. Styliaris, M. Kumari, and P. Zanardi, *Phys. Rev. Research* **3**, 023214 (2021).

[36] J. Cornelius, Z. Xu, A. Saxena, A. Chenu, and A. del Campo, (2021), arXiv:2108.06784 [quant-ph].

[37] F. Borgonovi, F. M. Izrailev, L. F. Santos, and V. G. Zelevinsky, *Physics Reports* **626**, 1 (2016).

[38] L. Leviandier, M. Lombardi, R. Jost, and J. P. Pique, *Phys. Rev. Lett.* **56**, 2449 (1986).

[39] J. Wilkie and P. Brumer, *Phys. Rev. Lett.* **67**, 1185 (1991).

[40] Y. Alhassid and N. Whelan, *Phys. Rev. Lett.* **70**, 572 (1993).

[41] J.-Z. Ma, *Journal of the Physical Society of Japan* **64**, 4059 (1995).

[42] E. Dyer and G. Gur-Ari, *J. High Energy Phys.* **2017**, 75 (2017).

[43] A. del Campo, J. Molina-Vilaplana, and J. Sonner, *Phys. Rev. D* **95**, 126008 (2017).

[44] L. K. Joshi, A. Elben, A. Vikram, B. Vermersch, V. Galitski, and P. Zoller, *Phys. Rev. X* **12**, 011018 (2022).

[45] T. Can, *Journal of Physics A: Mathematical and Theoretical* **52**, 485302 (2019).

[46] S. Denisov, T. Laptyeva, W. Tarnowski, D. Chruściński, and K. Życzkowski, *Phys. Rev. Lett.* **123**, 140403 (2019).

[47] L. Sá, P. Ribeiro, T. Can, and T. c. v. Prosen, *Phys. Rev. B* **102**, 134310 (2020).

[48] W. Tarnowski, I. Yusipov, T. Laptyeva, S. Denisov, D. Chruściński, and K. Życzkowski, *Phys. Rev. E* **104**, 034118 (2021).

[49] L. Sá, P. Ribeiro, and T. Prosen, “Lindbladian dissipation of strongly-correlated quantum matter,” (2021), arXiv:2112.12109 [cond-mat.stat-mech].

[50] G. Styliaris, N. Anand, and P. Zanardi, *Phys. Rev. Lett.* **126**, 030601 (2021).

[51] Z. Xu and A. del Campo, *Phys. Rev. Lett.* **122**, 160602 (2019).

[52] D. Poulin, R. Laflamme, G. J. Milburn, and J. P. Paz, *Phys. Rev. A* **68**, 022302 (2003).

[53] H. T. Quan, Z. Song, X. F. Liu, P. Zanardi, and C. P. Sun, *Phys. Rev. Lett.* **96**, 140604 (2006).

[54] J. Zhang, X. Peng, N. Rajendran, and D. Suter, *Phys. Rev. Lett.* **100**, 100501 (2008).

[55] R. Dorner, S. R. Clark, L. Heaney, R. Fazio, J. Goold, and V. Vedral, *Phys. Rev. Lett.* **110**, 230601 (2013).

[56] L. Mazzola, G. De Chiara, and M. Paternostro, *Phys. Rev. Lett.* **110**, 230602 (2013).

[57] T. B. Batalhão, A. M. Souza, L. Mazzola, R. Auccaise, R. S. Sarthour, I. S. Oliveira, J. Goold, G. De Chiara, M. Paternostro, and R. M. Serra, *Phys. Rev. Lett.* **113**, 140601 (2014).

[58] B.-B. Wei and R.-B. Liu, *Phys. Rev. Lett.* **109**, 185701 (2012).

[59] X. Peng, H. Zhou, B.-B. Wei, J. Cui, J. Du, and R.-B. Liu, *Phys. Rev. Lett.* **114**, 010601 (2015).

[60] A. Francis, D. Zhu, C. Huerta Alderete, S. Johri, X. Xiao, J. K. Freericks, C. Monroe, N. M. Linke, and A. F. Kemper, *Science Advances* **7**, 2447 (2021).

[61] B. Swingle, G. Bentsen, M. Schleier-Smith, and P. Hayden, *Phys. Rev. A* **94**, 040302 (2016).

[62] Y. Liu, J. Tian, R. Betzholz, and J. Cai, *Phys. Rev. Lett.* **122**, 110406 (2019).

[63] D. V. Vasilyev, A. Grankin, M. A. Baranov, L. M. Sieberer, and P. Zoller, *PRX Quantum* **1**, 020302 (2020).

[64] K. Papadodimas and S. Raju, *Phys. Rev. Lett.* **115**, 211601 (2015).

[65] G. Livan, M. Novaes, and P. Vivo, *Introduction to Random Matrices: Theory and Practice* (Springer, 2018).

[66] A. Chenu, J. Molina-Vilaplana, and A. del Campo, *Quantum* **3**, 127 (2019).

[67] J. Liu, *Phys. Rev. D* **98**, 086026 (2018).

[68] Y. Liu, M. A. Nowak, and I. Zahed, *Physics Letters B* **773**, 647 (2017).

[69] N. Hunter-Jones and J. Liu, *J. High Energy Phys.* **2018**, 202 (2018).

[70] A. Prakash, J. H. Pixley, and M. Kulkarni, *Phys. Rev. Research* **3**, L012019 (2021).

[71] T. Tkocz, M. Smaczyński, M. Kuś, O. Zeitouni, and K. Życzkowski, *Random Matrices: Theory and Applications* **01**, 1250009 (2012).

[72] S. C. L. Srivastava, S. Tomsovic, A. Lakshminarayanan, R. Ketzmerick, and A. Bäcker, *Phys. Rev. Lett.* **116**, 054101 (2016).

[73] X. Chen, R. Fan, Y. Chen, H. Zhai, and P. Zhang, *Phys. Rev. Lett.* **119**, 207603 (2017).

[74] X.-Y. Song, C.-M. Jian, and L. Balents, *Phys. Rev. Lett.* **119**, 216601 (2017).

[75] S.-K. Jian and H. Yao, *Phys. Rev. Lett.* **119**, 206602 (2017).

[76] J. Maldacena and X.-L. Qi, (2018), arXiv:1804.00491 [hep-th].

[77] A. M. García-García, T. Nosaka, D. Rosa, and J. J. M. Verbaarschot, *Phys. Rev. D* **100**, 026002 (2019).

[78] S. Plugge, E. Lantagne-Hurtubise, and M. Franz, *Phys. Rev. Lett.* **124**, 221601 (2020).

[79] X.-L. Qi and P. Zhang, *J. High Energy Phys.* **2020**, 129 (2020).

[80] S. Sahoo, E. Lantagne-Hurtubise, S. Plugge, and M. Franz, *Phys. Rev. Research* **2**, 043049 (2020).

[81] R. Haenel, S. Sahoo, T. H. Hsieh, and M. Franz, *Phys. Rev. B* **104**, 035141 (2021).

[82] T.-G. Zhou, L. Pan, Y. Chen, P. Zhang, and H. Zhai, *Phys. Rev. Research* **3**, L022024 (2021).

[83] S. Sachdev and J. Ye, *Phys. Rev. Lett.* **70**, 3339 (1993).

[84] A. Kitaev, Talks at The KITP on April 7 and May 27, 2015.

[85] I. Danshita, M. Hanada, and M. Tezuka, *Progress of Theoretical and Experimental Physics* **2017** (2017), 083I01.

[86] L. García-Álvarez, I. L. Egusquiza, L. Lamata, A. del Campo, J. Sonner, and E. Solano, *Phys. Rev. Lett.* **119**, 040501 (2017).

[87] D. I. Pikulin and M. Franz, *Phys. Rev. X* **7**, 031006 (2017).

[88] A. Chew, A. Essin, and J. Alicea, *Phys. Rev. B* **96**, 121119 (2017).

[89] Z. Luo, Y.-Z. You, J. Li, C.-M. Jian, D. Lu, C. Xu, B. Zeng, and R. Laflamme, *npj Quantum Information* **5**, 53 (2019).

[90] R. Babbush, D. W. Berry, and H. Neven, *Phys. Rev. A* **99**, 040301 (2019).

[91] C. Wei and T. A. Sedrakyan, *Phys. Rev. A* **103**, 013323 (2021).